International Journal of Rock Mechanics & Mining Sciences 47 (2010) 205–217

Contents lists available at ScienceDirect

International Journal of Rock Mechanics & Mining Sciences

journal homepage: www.elsevier.com/locate/ijrmms

# A fully coupled thermo-hydro-mechanical model for simulating multiphase flow, deformation and heat transfer in buffer material and rock masses

Fuguo Tong [a,*], Lanru Jing [a], Robert W. Zimmerman [b]

[a] Department of Land and Water Resources Engineering, Royal Institute of Technology, Stockholm, Sweden
[b] Department of Earth Science and Engineering, Imperial College, London, UK

ARTICLE INFO

*Article history:*
Received 8 November 2008
Received in revised form
31 October 2009
Accepted 13 November 2009
Available online 22 December 2009

*Keywords:*
Thermo-hydro-mechanical processes
Multiphase flow
Porous media
Buffer
FEM
Theory of mixtures
Radioactive waste repositories
Phase change
Relative humidity

ABSTRACT

This paper presents a numerical method for modeling coupled thermo-hydro-mechanical processes of geomaterials with multiphase fluid flow. A FEM code has been developed and validated for modeling the behavior of porous geological media, and is equally applicable for modeling coupled THM processes in rocks. The governing equations are based on the theory of mixtures applied to the multiphysics of porous media, considering solid phase deformation, multiphase fluid flow, and heat transport. New numerical techniques have been developed for more efficient FEM formulation and equation solution for modeling saturated or partially saturated water flow, gas flow and heat transfer in deformable porous media, as are commonly encountered in performance and safety assessment of underground radioactive repositories. The code has been validated against an experimental benchmark test, which involves bentonite under laboratory conditions, with good results. Several critical outstanding issues for modeling coupled processes of geomaterials are discussed in depth.



## 1. Introduction

Coupled thermo-hydro-mechanical (THM) processes are commonly simulated using the theories of porous media. The first such theory was Terzaghi's 1-D consolidation theory of soils [1], followed later by Biot's theory of isothermal consolidation of elastic porous media, a phenomenological approach of poroelasticity [2,3], and mixture theory as described by Morland [4], Bowen [5] and others. Non-isothermal consolidation of deformable porous media is the basis of modern coupled THM models, using either the averaging approach as proposed first by Hassanizadeh and Gray [6–9] and Achanta et al. [10], or an extension of Biot's phenomenological approach with a thermal component [11]. Both approaches are suitable for modeling coupled THM processes in geomaterials. In the early literature of coupled THM research, it was often stated that the theory of mixtures is more suitable for understanding the microscopic behavior of porous media, whereas poroelasticity theory is better suited for macroscopic description and computer modeling [12]. In this paper, we show that models based on the mixture theory can also be equally suitable for computer modeling when appropriate numerical techniques are used, and that these models show more flexibility for modeling unsaturated multiphase fluid flow in porous media.

In recent years, coupled thermo-hydro-mechanical behavior in porous media has been a subject of great interest in many engineering disciplines. Many attempts have been made to develop numerical prediction capabilities associated with topics such as the movement of pollutant plumes, gas injection, energy storage, permafrost and frozen soil engineering, safety assessment of waste repositories for radioactive waste and spent nuclear fuel, and geothermal energy extraction. Many computer codes have been applied in modeling coupled THM process, such as ROCMAS [13], THAMES [14], FRACON [15], ABAQUS [16], COMPASS [17] and CODE_BRIGHT [18]. Some of these codes can model fluid flow in unsaturated media by using Richard's equation [19], but gas movement is often not rigorously considered, since the gas pressure is assumed to be small and constant. The codes COMPASS and CODE_BRIGHT can simulate two-phase (gas and liquid) fluid flow with two components (air and water) in partially saturated soils, coupled with heat transport and mechanical response [20]. However, the advective flow of vapor was not well described, including heat transfer between the liquid and gas phases. As pointed out in [21], only if we consider the spontaneous thermo-dynamic equilibrium between the liquid water and the water vapor in the porous media, and treat the

* Corresponding author.
*E-mail address:* fuguo@kth.se (F.G. Tong).

1365-1609/$ - see front matter © 2009 Elsevier Ltd. All rights reserved.
doi:10.1016/j.ijrmms.2009.11.002

vapor pressure as a variable dependent on both suction and temperature, can the flux of vapor and liquid water be properly modeled using a single empirical equation [21,22]. Unfortunately, this approach makes it impossible to predict vapor pressure evolution accurately, and the relative humidity cannot be calculated according to its physical definition due to the limited validity of its empirical models. Another problem is that the porosity is often considered as a constant, or a simple function of bulk strain, in order to reduce the number of primary variables. This simplification can reduce the total number of equations, but may break the consistency among the three phases (solid, liquid and gas) and reduce the stability and efficiency of the numerical simulation.

The major objective of this paper is to present a more comprehensive modeling strategy for coupled THM processes and the numerical solution method for porous geomaterials. The work is part of work package 4 (WP4) of the THERESA project, which is supported by the European Commission. The objective of the project is to develop, verify and improve the modeling capabilities of coupled THM models and computer codes for performance and safety assessments of the safety of radioactive waste repositories. The main difference between the model proposed in this paper and other coupled THM numerical models mentioned above is that the gas flow and vapor flow processes are described explicitly by their mass conservation equations, so that phase change phenomena can be treated more objectively and efficiently. Another difference is that the mass conservation equation of the solid phase considers porosity changes that occur with deformation. Most importantly, an efficient equation solution strategy is developed to obtain stable and efficient numerical simulations, which is often the most challenging issue for modeling coupled THM processes with FEM, due to intrinsic numerical ill-conditioning caused by the coupling terms between the phases.

In the following sections, the general conservation equations and assumptions are first introduced, followed by development of the numerical model. The FEM formulation and solution strategy is introduced in the third section. The numerical results for the code (named ROLG) verification against a benchmark test problem as defined in WP4 of the THERESA project are presented afterwards, to verify the presented model and method. The paper is completed with a discussion section about outstanding issues and scientific conclusions.

## 2. General assumptions and basic conservation equations

### 2.1. General assumptions

Based on the theory of mixtures, a number of assumptions have been adopted to develop the coupled thermo-hydro-mechanical model for deformable porous geological media. Four of them of particular interest are:

(1) The partially saturated medium is treated as a multiphase system (solid, liquid, and gas). The voids of the solid skeleton are filled partially with liquid water, and partially with gas. The gas phase is modeled as an ideal gas mixture composed of dry air and water vapor. The liquid phase consists of water and dissolved air.
(2) The multiphase medium is considered as a mixture. Every phase is continuous and each spatial point in the mixture is assumed to be occupied simultaneously by a material point of every phase. The balance laws for the mixture as a whole have the same form as the equations for the balance laws of a single-phase material [23].
(3) The mechanical behavior of the multiphase medium considers the gas, liquid and solid responses to local pressure and the overall responses to the effective stresses.
(4) The fluid flow is a multiphase flow in a deformable porous medium under non-isothermal conditions.

### 2.2. Basic conservation equations—general forms

The unsaturated medium, in the context of theory of mixtures, is viewed as a mixed continuum of three independent overlapping phases [24]. For every phase, its conservation equation can be obtained according to principles of continuum mechanics and mixture theory, as can be found in [24–27].

#### 2.2.1. Mass conservation equation

Given an arbitrary spatial volume $V$, the time rate of change of the total mass of the $\alpha$ phase in $V$ must be equal to the flux of that phase across the boundary $\Gamma_V$ of $V$, plus the source $Q^\alpha$. This is the same as for a single-phase material, and the balance law for the $\alpha$ phase is

$$\frac{d}{dt}\int_V \rho^\alpha \, dV = -\int_{\Gamma_V} \rho^\alpha \mathbf{v}_\alpha \cdot \mathbf{n} \, dS + \int_V Q^\alpha \, dV \tag{1}$$

where $\rho^\alpha$ is the apparent mass density of the $\alpha$ phase, $\mathbf{v}_\alpha$ denotes the velocity field of particles of phase $\alpha$, $\Gamma_V$ is the boundary of $V$, and $\mathbf{n}$ is the unit outward normal vector to the boundary. Using the divergence theorem in the usual manner, one obtains the following local form of the balance law:

$$D_t^\alpha \rho^\alpha + \rho^\alpha \nabla \cdot \mathbf{v}_\alpha - Q^\alpha = 0 \tag{2}$$

where the material derivative relative to the $\alpha$ phase is given by

$$D_t^\alpha (\cdot) = \partial_t (\cdot) + \nabla (\cdot) \cdot \mathbf{v}_\alpha \tag{3a}$$

The velocity $\mathbf{v}_\alpha$ is related to the position vector $\mathbf{x}^\alpha$, and is written as

$$\mathbf{v}_\alpha = \partial_t \mathbf{x}^\alpha (\mathbf{X}^\alpha, t)|_{\mathbf{X}^\alpha} \tag{3b}$$

where $\mathbf{X}^\alpha$ is a material point for the $\alpha$ phase. For any spatial point $\mathbf{x}$ in the mixture, each phase must have a material point $\mathbf{X}^\alpha$ to occupy $\mathbf{x}$. The apparent density of $\alpha$ phase is expressed as

$$\rho^\alpha = \rho_\alpha \phi^\alpha \tag{3c}$$

where $\rho_\alpha$ and $\phi^\alpha$, respectively, denote the intrinsic density and the volume fractions of phase $\alpha$.

Inserting Eqs. (3a–c) into Eq. (2), the mass balance equation for $\alpha$ phase takes the form

$$\partial_t (\rho_\alpha \phi^\alpha) + \nabla \cdot (\mathbf{v}_\alpha \rho_\alpha \phi^\alpha) - Q^\alpha = 0 \tag{4}$$

#### 2.2.2. Momentum conservation equation

The conservation of linear momentum for the $\alpha$ phase of the mixture is the same as that for a single-phase material. In any given spatial volume $V$ of boundary $\Gamma_v$, the balance of linear momentum for the $\alpha$ phase (assuming no chemical reactions) [25] is written as

$$\frac{d}{dt}\int_V \rho^\alpha \mathbf{v}_\alpha \, dV = -\int_{\Gamma_V} \rho^\alpha \mathbf{v}_\alpha (\mathbf{v}_\alpha \cdot \mathbf{n}) \, dS + \int_{\Gamma_V} \boldsymbol{\sigma}^\alpha \cdot \mathbf{n} \, dS + \int_V \rho^\alpha \mathbf{b}_\alpha \, dV + \rho^\alpha \hat{\boldsymbol{\pi}}^\alpha \, dV \tag{5}$$

where $\boldsymbol{\sigma}^\alpha$ is the partial Cauchy stress tensor of the $\alpha$ phase. Note that $\int_{\Gamma_V} \boldsymbol{\sigma}^\alpha \cdot \mathbf{n} \, dS$ represents the contact force per unit area of the $\alpha$ phase in $V$, resulting from contact with the $\alpha$ phase outside $V$. The term $\mathbf{b}_\alpha$ is the body force per unit mass of the $\alpha$ phase. Symbol $\hat{\boldsymbol{\pi}}^\alpha$ is the momentum supply to phase $\alpha$ by the rest of the mixture. Using the divergence theorem again in the usual manner, and recalling Eq. (2), one obtains the following local form of the

momentum conservation equation:

$$\rho^{\alpha}\partial_t \mathbf{v}_{\alpha}+\rho^{\alpha}(\nabla \mathbf{v}_{\alpha})\cdot \mathbf{v}_{\alpha}=\nabla\cdot \boldsymbol{\sigma}^{\alpha}+\rho^{\alpha}\mathbf{b}_{\alpha}+\hat{\boldsymbol{\pi}}^{\alpha} \tag{6}$$

The momentum supplies should satisfy the constraint condition [28]

$$\sum_{\alpha=s,l,g}\hat{\boldsymbol{\pi}}^{\alpha}=0 \tag{7}$$

Summing up the momentum equation of the three phases, and accounting for Eq. (7), yields

$$\sum_{\alpha=s,l,g}\rho^{\alpha}\partial_t \mathbf{v}_{\alpha}+\sum_{\alpha=s,l,g}\rho^{\alpha}(\nabla \mathbf{v}_{\alpha})\cdot \mathbf{v}_{\alpha}=\nabla\cdot(\boldsymbol{\sigma}^{s}+\boldsymbol{\sigma}^{l}+\boldsymbol{\sigma}^{g})+\sum_{\alpha=s,l,g}\rho^{\alpha}\mathbf{b}_{\alpha} \tag{8}$$

#### 2.2.3. Heat energy conservation equation

Given any spatial volume $V$, the time rate of change of the total internal energy of phase $\alpha$ in $V$ must be equal to the heat flux of that phase across the boundary of $V$, $\Gamma_v$, plus the heat source $Q_T^{'\alpha}$, which is the $\alpha$ phase heat supply within the volume, and plus the energy supply $\hat{\varepsilon}^{\alpha}$ to the $\alpha$ phase due to the interactions with the other phase [24,25]. The heat energy conservation equation can then be written as

$$\frac{d}{dt}\int_V E_T^{\alpha}dV=-\int_{\Gamma_V}\mathbf{q}^{\alpha}\cdot\mathbf{n}\,dS+\int_V Q_T^{'\alpha}\,dV+\int_V\hat{\varepsilon}^{\alpha}\,dV \tag{9}$$

In a differential form, this relation may be expressed by

$$D_t E_T^{\alpha}=-\nabla\cdot\mathbf{q}^{\alpha}+Q_T^{'\alpha}+\hat{\varepsilon}^{\alpha} \tag{10}$$

where $E_T^{\alpha}$ is the total internal energy of phase $\alpha$ in $V$, and can be expressed as

$$E_T^{\alpha}=\rho^{\alpha}c_{\alpha}T_{\alpha} \tag{11a}$$

where $c_{\alpha}$ is the specific heat of the $\alpha$ phase, and $T_{\alpha}$ is the temperature of the $\alpha$ phase.

Generally, the heat flux vector $\mathbf{q}^{\alpha}$ can include heat conduction, convection and heat radiation terms. Here we only consider heat conduction and convection. The heat flux vector $\mathbf{q}^{\alpha}$ can be expressed as

$$\mathbf{q}^{\alpha}=-\mathbf{k}_{\alpha T}(\nabla T)+\rho^{\alpha}c_{\alpha}T_{\alpha}\mathbf{v}_{\alpha} \tag{11b}$$

where $\mathbf{k}_{\alpha T}$ is the thermal conductivity tensor of $\alpha$ phase.

The heat source $Q_T^{'\alpha}$ in Eqs. (9) and (10) is expressed as

$$Q_T^{'\alpha}=Q_T^{\alpha}+Q1_T^{\alpha}-Q2_T^{\alpha} \tag{11c}$$

where $Q_T^{\alpha}$ is the other heat potential sources that may occur from the other physical or chemical processes, such as electric or magnetic processes and chemical reactions. Symbol $Q1_T^{\alpha}$ represents the heat energy that is produced by the work by external forces. For elastic behavior, it is always equal to zero. Symbol $Q2_T^{\alpha}$ is the heat energy reduction due to thermal power in the course of the bulk deformation, and is expressed as

$$Q2_T^{\alpha}=K_{\alpha}\beta_{\alpha}T_{\alpha}(\nabla\cdot\mathbf{v}_{\alpha}) \tag{11d}$$

where $K_{\alpha}$ is the bulk modulus, and $\beta_{\alpha}$ is the coefficient of volumetric thermal expansion. The unit of temperature is Kelvin.

Substituting Eqs. (11a–d) into Eq. (10), the heat energy conservation equation for the $\alpha$ phase is obtained as

$$D_t(\rho^{\alpha}c_{\alpha}T_{\alpha})=\nabla\cdot[\mathbf{k}_{\alpha T}(\nabla T_{\alpha})]-\nabla\cdot(\mathbf{v}_{\alpha}\rho^{\alpha}c_{\alpha}T_{\alpha})-K_{\alpha}\beta_{\alpha}T_{\alpha}\nabla\cdot\mathbf{v}_{\alpha}+Q_T^{\alpha}+\hat{\varepsilon}^{\alpha} \tag{12}$$

Note that the energy supply $\hat{\varepsilon}^{\alpha}$ in Eq. (10) must obey the following condition:

$$\hat{\varepsilon}^{g}+\hat{\varepsilon}^{l}+\hat{\varepsilon}^{s}=0 \tag{13}$$

Summing up heat energy equation of the three phases, accounting for Eq. (12), yields

$$\sum_{\alpha=s,l,g}D_t(\rho^{\alpha}c_{\alpha}T_{\alpha})-\sum_{\alpha=s,l,g}\nabla\cdot[\mathbf{k}_{\alpha T}(\nabla T_{\alpha})]+\sum_{\alpha=s,l,g}\nabla\cdot(\mathbf{v}_{\alpha}\rho^{\alpha}c_{\alpha}T_{\alpha})+\sum_{\alpha=s,l,g}K_{\alpha}\beta_{\alpha}T_{\alpha}(\nabla\cdot\mathbf{v}_{\alpha})-\sum_{\alpha=s,l,g}Q_T^{\alpha}=0 \tag{14}$$

## 3. Numerical model development

### 3.1. Deformation model: the mechanical process

#### 3.1.1. Static equilibrium equation

Adopting the assumption of small the deformation and the assumption of small velocity, then $\mathbf{v}_{\alpha}\approx\mathbf{0}$, Eq. (8) can be simplified to

$$\nabla\cdot(\boldsymbol{\sigma}^{s}+\boldsymbol{\sigma}^{l}+\boldsymbol{\sigma}^{g})+\sum_{\alpha=s,l,g}\rho^{\alpha}\mathbf{b}_{\alpha}=0 \tag{15}$$

According to the concept of effective stress and mixture theory [25,29–35], one has the following expressions:

$$\boldsymbol{\sigma}^{s}=\boldsymbol{\sigma}-\phi^{s}\alpha_B[S_r p_l+(1-S_r)p_g]\boldsymbol{I}-K\beta T\boldsymbol{I}-K\varepsilon'\boldsymbol{I} \tag{16a}$$

$$\boldsymbol{\sigma}^{l}=-\phi^{l}\alpha_B p_l\boldsymbol{I} \tag{16b}$$

$$\boldsymbol{\sigma}^{g}=-\phi^{g}\alpha_B p_g\boldsymbol{I} \tag{16c}$$

where $\boldsymbol{\sigma}$ is the total stress tensor, $K$ is the bulk modulus of the skeleton, $\beta$ is the volumetric thermal expansion coefficient, and $S_r$ is the degree of saturation, respectively. The variables $p_g$, $p_l$ and $T$ are the gas pressure, liquid pressure and temperature, respectively, $\varepsilon'$ is the swelling volumetric strain of the solid skeleton, $\boldsymbol{I}$ is the identity tensor, $K_S$ is the bulk modulus of the solid constituent, and $\alpha_B=1-K/K_S$ is the Biot coefficient.

Here, traditional effective stress should be $\sigma^{s}+\sigma^{l}+\sigma^{g}=\sigma'$, so according to Eq. (16), the effective stress can be written as: $\sigma-\alpha_B p_g\boldsymbol{I}+S_r\alpha_B(p_g-p_l)\boldsymbol{I}-K\beta T\boldsymbol{I}-K\varepsilon'\boldsymbol{I}$. For a fully saturated condition (ignoring the temperature and swelling strain terms), it can be rewritten as $\sigma-\alpha_B p_l\boldsymbol{I}$, which is Terzaghi's effective stress.

Substituting Eqs. (16a–c) into Eq. (15), and considering $\boldsymbol{\sigma}=\mathbf{D}:\nabla\mathbf{u}$, $\phi^{l}=(1-\phi^{s})S_r$ and $\phi^{g}=(1-\phi^{s})(1-S_r)$, the static equilibrium equation can be obtained as

$$\nabla\cdot[\mathbf{D}:\nabla\mathbf{u}-\alpha_B p_g\boldsymbol{I}+S_r\alpha_B(p_g-p_l)\boldsymbol{I}-K\beta T\boldsymbol{I}-K\varepsilon'\boldsymbol{I}]+\sum_{\alpha=s,l,g}\rho^{\alpha}\mathbf{b}_{\alpha}=0 \tag{17}$$

where $\mathbf{u}$ is the total displacement vector, and $\mathbf{D}$ is the elastic modulus tensor of the underlying drained solid.

Defining $\chi=S_r\alpha_B$, and considering $\alpha_B p_g\approx p_g$, Eq. (17) can be rewritten in time derivative form as

$$\nabla\cdot\left(\mathbf{D}:\nabla\frac{\partial\mathbf{u}}{\partial t}\right)-\nabla\cdot\left[(1-\chi)\frac{\partial p_g}{\partial t}\boldsymbol{I}\right]-\nabla\cdot\left[\chi\frac{\partial p_l}{\partial t}\boldsymbol{I}\right]-\nabla\cdot\left[K\beta\frac{\partial T}{\partial t}\boldsymbol{I}\right]-\nabla\cdot\left[K\frac{\partial\varepsilon'}{\partial t}\boldsymbol{I}\right]+\frac{\partial\mathbf{F}_b}{\partial t}=0 \tag{18}$$

where $\chi$ is called Bishop's effective stress parameter, and $\mathbf{F}_b=\sum_{\alpha=s,l,g}\rho^{\alpha}\mathbf{b}_{\alpha}$. For the purposes of numerical simulation, Bishop's parameter is usually considered to be an experimental parameter, and more complicated models are used instead of $\chi=S_r\alpha_B$. This is because the real porous medium cannot strictly meet the assumptions introduced in this paper. Particularly in the unsaturated state, significant discrepancies may occur if Bishop's parameter is simply considered to be a linear function of the saturation degree.

*3.1.2. Constitutive models and material parameters*

*Stress–strain relation*: The stress–strain behavior of partially saturated soils is a complicated issue, and numerous stress–strain models have been developed. One of them, the Barcelona basic model (BBM), is an elastoplastic model which has been widely cited for developing new models [36]. In the present paper, a simple nonlinear elastic model is introduced for the simulation of the benchmark tests. The elastic model represents isotropic and homogeneous elastic behavior characterized by two elastic constants, the bulk modulus and shear modulus. For the elasticity constants, a nonlinear stress–strain relation is adopted [37]:

$$\varepsilon_b = \kappa \ln(\overline{\sigma}/\sigma_{ref}) \tag{19a}$$

where $\sigma_{ref}$ is the isotropic reference stress, $\overline{\sigma}$ the effective mean-stress, $\varepsilon_b$ the volumetric strain, and $\kappa$ is a compliance coefficient. The bulk modulus can be obtained as

$$K = \frac{d\overline{\sigma}}{d\varepsilon_b} = \frac{\overline{\sigma}}{\kappa} \tag{19b}$$

The shear modulus $G$ is related to the bulk modulus $K$ and Poisson's ratio $\nu$ through

$$G = K\frac{3(1-2\nu)}{2(1+\nu)} \tag{19c}$$

In the simulation presented in this paper, the compliance coefficient $\kappa$ and Poisson's ratio $\nu$ were taken to be 0.0024 and 0.3, respectively.

*Bishop's parameter*: The definition of Bishop's parameter is motivated by experimental and theoretical arguments. Bishop's parameter describes the contribution of matric suction to the effective stress; it may be regarded as a scaling factor averaging matric suction from a pore scale level to a macroscopic level over the representative elementary volume. Bishop's parameter is usually taken to be a function of suction [38], and written as

$$\chi = 1 \text{ for } s \le s_e, \quad \chi = (s_e/s)^{0.55} \text{ for } s \ge s_e \tag{20a}$$

Considering the compressibility of the solid constituent, Bishop's parameter is given in the present work by

$$\chi = (1-K/K_s) \text{ for } s \le s_e, \quad \chi = (1-K/K_s)(s_e/s)^{0.55} \text{ for } s \ge s_e \tag{20b}$$

where $K_S$ is the bulk modulus of the solid constituent, $K$ the drained bulk modulus, and $s$ is the suction. Symbol $s_e$ is the minimal suction (air entry value at which the air enters the pores), and it was set as 1.0 kPa in the simulation presented later.

*Swelling strain*: The swelling strain depends on the type of soil, as different soils have completely different swelling behaviors. For clay, some swelling models are available [39–42]. According to the properties of MX-80 bentonite [43], an empirical formula for the swelling strain of bentonite can be written in terms of the suction, $s$, as

$$\varepsilon' = -0.00015 \ln(s) \tag{21}$$

### 3.2. Liquid flow model—the liquid phase transport process

*3.2.1. Liquid flow equation*

Neglecting inertial and viscous effects, the advective flux of liquid phase includes a pressure driving component and a thermo-osmosis component, expressed as

$$\mathbf{v}_l^r = -\frac{k_l^r \mathbf{k}}{\mu_l}(\nabla p_l + \rho_l \mathbf{g}) - \mathbf{k}_T^l \nabla T \tag{22a}$$

where $\mathbf{k}$ is the intrinsic permeability tensor, $\mu_l$ is the fluid viscosity, $k_l^r$ is the liquid relative permeability, $\mathbf{g}$ is the gravitational acceleration vector, and $k_T^l$ is the coefficient of thermal coupling for liquid flux. The relative velocity of liquid can also be written as

$$\mathbf{v}_l^r = \phi^l(\mathbf{v}_l - \mathbf{v}_s) \tag{22b}$$

Substituting Eq. (22a) into Eq. (22b) yields

$$\mathbf{v}_l = \frac{1}{\phi^l}\left[-\frac{k_l^r \mathbf{k}}{\mu_l}(\nabla p_l + \rho_l \mathbf{g}) - \mathbf{k}_T^l \nabla T\right] + \mathbf{v}_s \tag{23}$$

where $\phi^l$ is the volumetric liquid content. Considering the solubility of gas in liquid, the volumetric liquid content can be expressed by

$$\phi^l = n\frac{\rho_l(1+H)S_r - \rho_v}{\rho_l - \rho_v} \equiv nS_{re} \tag{24}$$

where $n$ is the porosity, $\rho_v$ is the density of the vapor, $H$ is the coefficient of solubility of gas in liquid defined by Henry's law, and $S_r$ is the degree of saturation defined as the volume of water divided by the volume of void space, and can be expressed as

$$S_r = \frac{\phi^l \rho_l + \phi^g \rho_v}{\rho_l(1+H)n} \tag{25}$$

Considering only the rate of moisture transfer between the liquid and the gas phases as the source term, according to Dalton's equation the phase change flux can be described as

$$q_p = \rho_l \omega(p_{sv} - p_v) \tag{26}$$

where $\omega > 0$ is the liquid phase transfer coefficient, $p_v$ is the vapor pressure, and $p_{sv}$ is the saturated vapor pressure. The phase change flux $q_p$ is negative for condensation and positive for vaporization.

Substituting Eqs. (23), (24), and (26) into Eq. (4), and neglecting the smaller terms, the differential equation governing the non-isothermal liquid flow through an unsaturated porous medium is obtained finally as follows:

$$C_T^l \frac{\partial T}{\partial t} + C_g^l \frac{\partial p_g}{\partial t} + C_l^l \frac{\partial p_l}{\partial t} + C_m^l \nabla \cdot \frac{\partial \mathbf{u}}{\partial t} + S_{re}\frac{\partial n}{\partial t} - \nabla \cdot \left[\frac{k_l^r \mathbf{k}}{\mu_l}(\nabla p_l + \rho_l \mathbf{g})\right] - \nabla \cdot (\mathbf{k}_T^l \nabla T) + \omega(p_{sv} - p_v) = 0 \tag{27}$$

where the coefficients in the above equation are defined as follows:

$$C_T^l = -nS_{re}\beta_l \tag{28a}$$

$$C_g^l = \frac{n\partial S_{re}}{\partial s} \tag{28b}$$

$$C_l^l = \frac{nS_{re}}{K_l} - \frac{n\partial S_{re}}{\partial s} \tag{28c}$$

$$C_m^l = nS_{re} \tag{28d}$$

where $s$ is the suction, $\beta_l$ is the volumetric thermal expansion coefficient, $K_l$ is the bulk modulus of liquid phase, and the other coefficients are as defined previously.

*3.2.2. Constitutive models and material parameters*

*Water retention curve*: The water retention curve is a basic hydrophysical property of porous media, and can be described by the dependence between water content and water potential. Many water retention models have been proposed [44–48]. In this study, the relation between suction and degree of saturation is

defined by an empirical water retention curve, expressed by [49]

$$S_r = \rho_d\left(0.1096\frac{1}{n}+0.4189\right) \times\left[1+\left\{\frac{s}{12.68\exp[-7.97(n-0.4)-0.00647(T-20)]}\right\}^{1/0.789}\right]^{-0.211} \quad (29)$$

where $\rho_d$ (=1.791 kg/m$^3$) is the dry density, $n$ is the porosity, and $T$ is the temperature. Note that hysteresis, which is treated in some models [45], is neglected in our model.

*Liquid relative permeability*: In this work, the relative permeability $k_r^l$ of water is assumed to be a function of the degree of saturation and the porosity, and is expressed by [50]

$$k_r^l = k_{rS}^l k_{rn}^l = \left(\frac{S_r-S_r^r}{1-S_r^r}\right)^3\left(\frac{n}{n_0}\right)^7 \quad (30)$$

where $S_r^r$ is a residual degree of water saturation, set to 0.001 in the simulation of benchmark test presented in this paper, and $n_0$ is the initial porosity. There are, of course, many other relative permeability models that could be implemented into our general model [51–53].

*Water density:* The density of water, $\rho_l$, is expressed here by

$$\rho_l = \rho_T\left[1-\frac{(p_l-101325.0)}{K_l}\right]^{-1} \quad (31)$$

where $\rho_T$=1000.066219+0. 0209229$T$−0.00602137$T^2$+0.0000163$T^3$ is the density at atmospheric pressure, in units of kg/m$^3$, $T$ is the temperature in °C, $K_l$ (=2.15 × 10$^9$ Pa) is the bulk modulus of water, and $p_l$ is the pressure, in Pa.

*The coefficient of solubility of gas in liquid*, $H$: According to Henry's law, at a constant temperature, the amount of a given gas dissolved in a given type and volume of liquid is directly proportional to the partial pressure of that gas in equilibrium with that liquid:

$$C = \frac{p}{k} \quad (32a)$$

where $C$ is the concentration of the gas solution in the liquid, $p$ is partial pressure of the gas over the liquid, and $k$ is the Henry's law constant, which is a function of temperature and can be expressed in a form of the Van't Hoff equation as

$$k(T) = k(T_\theta)\exp\left[-\eta\left(\frac{1}{T}-\frac{1}{T_\theta}\right)\right] \quad (32b)$$

where $T$ is the absolute temperature in K, $T_\theta$=298 K, and $k(T_\theta)$ is the Henry's law constant in units of L atm/mol, which is equal to 769.2 for oxygen and 1639.34 for nitrogen, when the liquid is water. The dimensionless coefficient $\eta$ is equal to 1700 for oxygen and 1300 for nitrogen. If the dry gas is only composed of oxygen and nitrogen, and the volume content is 0.2 and 0.8, respectively, as commonly assumed for air, then the coefficient of solubility of dry gas in water can be calculated, in units of g/L, as

$$C = C_{o_2}+C_{N_2} = (\lambda_{o_2}+\lambda_{N_2})(p_g-p_v) \quad (32c)$$

where $\lambda_{o_2} = 8.21\times10^{-8}\exp\{1700[(1/T)-(1/298)]\}$, and $\lambda_{N_2} = 1.35\times10^{-7}\exp\{1300[(1/T)-(1/298)]\}$. To be dimensionless, the coefficient $H$ can be obtained as

$$H = C/\rho_l = (\lambda_{o_2}+\lambda_{N_2})(p_g-p_v)\times10^{-3} \quad (33)$$

*Liquid (water) phase transfer coefficient*, $\omega$: The liquid water phase transfer coefficient $\omega>0$ is described by

$$\omega = C\frac{1}{\rho_l}\sqrt{\frac{M}{2\pi RT}} = 0.0185668\frac{C}{\rho_l\sqrt{T}} \quad (34)$$

where $C$ is an accommodation coefficient, which was set to 0.00002 in the simulation presented in this paper. The parameter $\omega$ has units of ms/kg.

*Saturated vapor pressure*: The saturated vapor pressure can be obtained using the psychrometric law [54]

$$p_{sv} = p_{svo}\exp(-sM_l/\rho_l RT) \quad (35a)$$

where $M_l$=0.018 kg/mol is the molecular mass of the liquid, $R$=8.314 J mol$^{-1}$ K$^{-1}$ is the universal gas constant, and $s$ is the suction, in units of Pa. Symbol $p_{svo}$ is the saturated vapor pressure in contact with the liquid over a planar surface, which can be obtained (in units of Pa) from the Clausius–Clapeyron equation [55], as

$$p_{svo} = 101325\times\exp\{-4895.36[(1/T)-(1/373)]\} \quad (35b)$$

Substituting Eq. (35b) into Eq. (35a) yields

$$p_{sv} = 101,325\exp\left[-4895.36\left(\frac{1}{T}-\frac{1}{373}\right)-0.002165\frac{s}{\rho_l T}\right] \quad (36)$$

*Viscosity of water*: The viscosity of water can be expressed as [56]

$$\mu_l = 1.984\times10^{-6}\exp(1825.85/T) \quad (37)$$

where the viscosity is in units of N s/m$^2$, and $T$ is in Kelvin.

### 3.3. Gas flow model—the gas phase transport process

#### 3.3.1. Gas flow equation

The gas phase is a mixture of dry air and water vapor. Its averaged advective velocity with respect to the solid phase is due to the gas pressure and temperature gradients, and is written as

$$\mathbf{v}_g^r = -\frac{k_g^r\mathbf{k}}{\mu_g}(\nabla p_g+\rho_g\mathbf{g})-\mathbf{k}_T^g\nabla T \quad (38a)$$

where $\mathbf{k}$ is the intrinsic permeability, $\mu_g$ is the viscosity of gas, $k_g^r$ is the gas relative permeability, $\rho_g$ is the density of gas, and $\mathbf{g}$ is the gravitational acceleration vector. Symbol $\mathbf{k}_T^g$ is the coefficient of thermal coupling for gas flux. The relative velocity of gas can also be expressed as

$$\mathbf{v}_g^r = \phi^g(\mathbf{v}_g-\mathbf{v}_s) \quad (38b)$$

Substituting Eq. (38a) into Eq. (38b) yields

$$\mathbf{v}_g = \frac{1}{\phi^g}\left[-\frac{k_g^g\mathbf{k}}{\mu_g}(\nabla p_g+\rho_g g)-\mathbf{k}_T^g\nabla T\right]+\mathbf{v}_s \quad (39)$$

Substituting Eq. (39) into Eq. (4), and neglecting the smaller terms, the equation of gas flow in porous media is obtained as follows:

$$C_T^g\frac{\partial T}{\partial t}+C_g^g\frac{\partial p_g}{\partial t}+C_l^g\frac{\partial p_l}{\partial t}+C_m^g\nabla\cdot\frac{\partial\mathbf{u}}{\partial t}+C_n^g\frac{\partial n}{\partial t} -\nabla\cdot\left[\frac{k_g^r\mathbf{k}}{\mu_g}(\nabla p_g+\rho_g\mathbf{g})\right]-\nabla\cdot[\mathbf{k}_T^g\nabla T]-\omega(p_{sv}-p_v)=0 \quad (40)$$

where $\mu_g$ is the gas viscosity, $k_g^r$ is the gas relative permeability, and the other coefficients are defined as follows:

$$C_T^g = -\frac{n(1-S_{re})}{T} \quad (41a)$$

$$C_g^g = \frac{n(1-S_{re})}{p_g}-\frac{n\partial S_{re}}{\partial s} \quad (41b)$$

$$C_l^g = \frac{n\partial S_{re}}{\partial s} \quad (41c)$$

$$C_m^g = n(1-S_{re}) \quad (41d)$$

$$C_n^g = 1-S_{re} \quad (41e)$$

#### 3.3.2. Constitutive models and material parameters

*Relative permeability of gas*: In this study, the relative permeability of gas, $k_g^r$, is assumed to be a function of the degree of saturation only, expressed by [57]

$$k_g^r = \left[1-\left(\frac{S_r-S_r^r}{1-S_r^r}\right)\right]^3 \tag{42}$$

Other available relative permeability models [58–60] could also be used.

*Water vapor density*: According to the state equation of gas, which is $\rho = p/RT$, where $T$ is the absolute temperature, and with the gas constant $R$=462.5 J kg$^{-1}$ K$^{-1}$, the density of the vapor can be expressed in units of kg/m$^3$ as

$$\rho_v = 0.0021668(p_v/T) \tag{43}$$

*Gas density*: The gas is a mixture of dry air and vapor. Here we assume that the dry gas is only made up of oxygen and nitrogen, and their pressures are given by $p_{o_2} = 0.2(p_g - p_v)$, and $p_{N_2} = 0.8(p_g - p_v)$. According to the state equation of gas, the density of gas can be obtained as

$$\rho_g = 0.00346524(p_g/T) - 0.00129844(p_v/T) \tag{44}$$

where density is in units of kg/m$^3$, pressure is in Pa, and temperature is in Kelvin.

*Gas viscosity*: The viscosity of gas, $\mu_g$, is computed using Sutherland's formula [61]:

$$\mu_g = \mu_0\left(\frac{0.999T_0+c}{0.999T+c}\right)\left(\frac{T}{T_0}\right)^{1.5} \tag{45}$$

For standard air, $c$=120, $T_0$=291.15, and $\mu_0$=0.00001827, where $T$ is in Kelvin, and viscosity is in units of N s/m$^2$.

### 3.4. Vapor flow model—the gas phase transport process

#### 3.4.1. Vapor flow equation

The vapor is mixed with other gases, so the volumetric content of vapor should be equal to that of gases, i.e., $\phi^v = \phi^g$. The relative vapor velocity $\mathbf{v}_v^r$ includes both the relative velocity of the whole gas $\mathbf{v}_g^r$ and the relative velocity with respect to its moving components $\mathbf{v}_v^d$ because of molecular diffusion, i.e.

$$\mathbf{v}_v^r = \mathbf{v}_g^r + \mathbf{v}_v^d \tag{46a}$$

Following the Fickian concept of mass transport by molecular diffusion, the diffusive vapor relative velocity due to the vapor gradient is written as

$$\mathbf{v}_v^d = -\phi^v \mathbf{D}_{ve}\nabla p_v \tag{46b}$$

where $p_v$ is vapor pressure, and $\mathbf{D}_{ve}$ is the tensor of the molecular diffusivity of vapor, with units m$^2$/s Pa, and which can be expressed as

$$\mathbf{D}_{ve} = \boldsymbol{I} D_v \frac{1}{\rho_w RT} \tag{46c}$$

where $D_v$ is the molecular diffusivity of vapor in pore gas, with units of m$^2$/s, and $\rho_w$ is the water density.

The relative velocity of vapor is written as

$$\mathbf{v}_v^r = \phi^v(\mathbf{v}_v - \mathbf{v}_s) \tag{46d}$$

Similar to the derivation of the gas velocity, the velocity of vapor is finally obtained as

$$\mathbf{v}_v = \frac{1}{\phi^g}\left[-\frac{k_r^g \mathbf{k}}{\mu_g}(\nabla p_g + \rho_g \mathbf{g}) - \mathbf{k}_T^g \nabla T\right] - \mathbf{D}_{ve}\nabla p_v + \mathbf{v}_s \tag{47}$$

Substituting Eq. (47) into Eq. (4), and neglecting the smaller terms, the equation of vapor flow in the porous medium is obtained as

$$C_T^v\frac{\partial T}{\partial t} + C_v^v\frac{\partial p_v}{\partial t} + C_g^v\frac{\partial p_g}{\partial t} + C_l^v\frac{\partial p_l}{\partial t} + C_m^v\nabla\cdot\frac{\partial \mathbf{u}}{\partial t} + C_n^v\frac{\partial n}{\partial t} - \nabla\cdot\left[\frac{k_g^r \mathbf{k}}{\mu_g}(\nabla p_g + \rho_g \mathbf{g})\right] - \nabla\cdot[\mathbf{k}_T^g\nabla T] - \nabla\cdot(C_d^v \mathbf{D}_{ve}\nabla p_v) - \omega(p_{sv} - p_v) = 0 \tag{48}$$

The various coefficients are defined as follows:

$$C_T^v = -\frac{n(1-S_{re})}{T} \tag{49a}$$

$$C_v^v = \frac{n(1-S_{re})}{p_v} \tag{49b}$$

$$C_g^v = -\frac{n\partial S_{re}}{\partial s} \tag{49c}$$

$$C_l^v = \frac{n\partial S_{re}}{\partial s} \tag{49d}$$

$$C_m^v \equiv C_d^v = n(1-S_{re}) \tag{49e}$$

$$C_n^v = (1-S_{re}) \tag{49f}$$

### 3.5. Heat transport model

#### 3.5.1. Heat transport equation

It is assumed that the temperature of the solid, liquid and gas phases are in local thermal equilibrium, i.e., $T_s \equiv T_l \equiv T_g \equiv T$. The thermal conductivity of the medium is assumed to be the sum of the thermal conductivities of its component phases, as given by

$$\boldsymbol{k}_T \equiv \boldsymbol{k}_{sT} + \boldsymbol{k}_{lT} + \boldsymbol{k}_{gT} \tag{50a}$$

$$Q \equiv Q_T^s + Q_T^l + Q_T^g \tag{50b}$$

where $\boldsymbol{k}_T$ and $Q_T$ are the thermal conductivity tensor and heat source of the multiphase media, respectively.

Substituting Eqs. (23), (39), (50a, b) into Eq. (14), and neglecting the smaller terms, the differential equation governing heat transport through a unsaturated porous medium is obtained finally as follows:

$$C_c^T\frac{\partial T}{\partial t} - \nabla\cdot(\mathbf{C}_T^T\nabla T) - \nabla\cdot[\mathbf{C}_g^T(\nabla p_g + \rho_g \mathbf{g}\mathbf{C})] - \nabla\cdot[\mathbf{C}_l^T(\nabla p_l + \rho_l \mathbf{g})] + C_s^T\nabla\cdot\frac{\partial \mathbf{u}}{\partial t} - Q = 0 \tag{51}$$

where the coefficients are defined as follows:

$$C_c^T = (1-n)\rho_s c_s + nS_{re}\rho_l c_l + n(1-S_{re})\rho_g c_g \tag{52a}$$

$$C_T^T = k_T + \rho_l c_l T k_T^l + \rho_g c_g T k_T^g + K_l\beta_l T\frac{1}{nS_{re}}k_T^l + K_g\beta_g T\frac{1}{n(1-S_{re})}k_T^g \tag{52b}$$

$$C_g^T = \rho_g c_g T\frac{k_r^g k}{\mu_g} + K_g\beta_g T\frac{1}{n(1-S_{re})}\frac{k_r^g k}{\mu_g} \tag{52c}$$

$$C_l^T = \rho_l c_l T\frac{k_r^l k}{\mu_l} + K_l\beta_l T\frac{1}{nS_{re}}\frac{k_r^l k}{\mu_l} \tag{52d}$$

$$C_s^T = [(1-n)\rho_s c_s + \rho_l c_l + \rho_g c_g]T + 3K\beta T + K_l\beta_l T + K_g\beta_g T \tag{52e}$$

#### 3.5.2. Constitutive models and material parameters: heat transport

*Thermal conductivity*: The thermal conductivity $k_T$ depends on saturation, temperature and porosity. In this study, the thermal

conductivity $k_T$ of the MX-80 compacted bentonite, at laboratory temperature, is related to the degree of saturation $S_r$ through the following expression [43]:

$$k_T = 1.28 - \frac{0.71}{1+\exp(10S_r - 6.5)} \tag{53}$$

where $S_r$ is the degree of saturation, and $k_T$ is in units of W/m K. Several other thermal conductivity models are available for soils [62–66], and could be used if other media were being modeled with our code.

*Specific heat capacity of water*: The specific heat capacity of water, $c_l$, can be expressed as a function of temperature, as follows:

$$c_l = 6872.8945 - 23.090239T + 0.06893537T^2 - 0.000073503 65T^3 \tag{54}$$

where $T$ is in K, and $c_l$ is in units of J/kg.

*Specific heat capacity of gas*: Because the gas is a mixture of dry air and vapor, the specific heat capacity of gas, $c_g$, is calculated by

$$c_g = \frac{c_v\rho_v + c_{air}\rho_{air}}{\rho_v + \rho_{air}} \tag{55a}$$

Using the state equation of gas and introducing the physical constants of vapor and air, Eq. (55a) can be rewritten as

$$c_g = \frac{7p_g + p_v}{0.007p_g - 0.002666p_v} \tag{55b}$$

where $c_g$ is in units of J/kg.

*Thermal expansion coefficient of water*: The thermal expansion coefficient of water, $\beta_l$, is given as a function of temperature by

$$\beta_l = -0.0864565 + 9.8063\times10^{-4}T - 4.2088\times10^{-6}T^2 + 8.1167\times10^{-9}T^3 - 5.903\times10^{-12}T^4 \tag{56}$$

*Thermal expansion coefficient of gas*: The thermal expansion coefficient of gas, $\beta_g$, can be calculated by

$$\beta_g = -\frac{1}{\rho_g}\frac{\partial\rho_g}{\partial T} = \frac{1}{T} \tag{57}$$

*Bulk modulus of gas*: The bulk modulus of the gas, $K_g$, is expressed by

$$K_g = \left(\frac{1}{\rho_g}\frac{\partial\rho_g}{\partial p_g}\right)^{-1} = p_g \tag{58}$$

*Other parameters*: The water bulk modulus $K_l$ is equal to $2.15\times10^9$ Pa. For the bentonite used in the benchmark test of WP4 in the THERESA project, the solid phase specific heat is equal to $c_s$=920 J/kg.

### 3.6. Solid mass conservation equation

The consistency of the three phases (solid, liquid and gas) depends on the variation of porosities of each phase. Thus, a new governing equation involving variable porosity is needed, which can be obtained by considering the solid mass conservation under varying stress and fluid pressure. Here we assume that the density of the solid phase is a function of temperature, liquid pressure, gas pressure, and the effective mean-stress. This then leads to

$$\partial_t(\rho_s\phi^s) = \phi^s\left[\frac{\partial\rho_s}{\partial T}\frac{\partial T}{\partial t} + \frac{\partial\rho_s}{\partial p_l}\frac{\partial p_l}{\partial t} + \frac{\partial\rho_s}{\partial p_g}\frac{\partial p_g}{\partial t} + \frac{\partial\rho_s}{\partial\overline{\sigma}}\frac{\partial\overline{\sigma}}{\partial t}\right] + \rho_s\partial_t\phi^s \tag{59a}$$

and

$$\nabla\cdot(v_s\rho_s\phi^s) = \rho_s\phi^s\partial_t\varepsilon_b + v_{si}\phi^s\left(\frac{\partial\rho_s}{\partial T}\frac{\partial T}{\partial x_i} + \frac{\partial\rho_s}{\partial p_l}\frac{\partial p_l}{\partial x_i} + \frac{\partial\rho_s}{\partial p_g}\frac{\partial p_g}{\partial x_i} + \frac{\partial\rho_s}{\partial\overline{\sigma}}\frac{\partial\overline{\sigma}}{\partial x_i}\right) + v_{si}\rho_s\frac{\partial\phi^s}{\partial x_i} \tag{59b}$$

Substituting Eqs. (59a) and (59b) into Eq. (4), neglecting the smaller terms and the source term, yields

$$\phi^s\left[\frac{\partial\rho_s}{\partial T}\frac{\partial T}{\partial t} + \frac{\partial\rho_s}{\partial p_l}\frac{\partial p_l}{\partial t} + \frac{\partial\rho_s}{\partial p_g}\frac{\partial p_g}{\partial t} + \frac{\partial\rho_s}{\partial\overline{\sigma}}\frac{\partial\overline{\sigma}}{\partial t}\right] + \rho_s\partial_t\phi^s + \rho_s\phi^s\partial_t\varepsilon_b + v_{si}\rho_s\frac{\partial\phi^s}{\partial x_i} = 0 \tag{60}$$

where $v_{si}$ is the velocity of solid phase in the $i$th direction. Because $\phi^s = 1-n$, and $v_{si} = \partial u_i/\partial t$, the above equation can be written as

$$\beta_s\frac{\partial T}{\partial t} + \frac{1}{\rho_s}\left[\frac{\partial\rho_s}{\partial p_l}\frac{\partial p_l}{\partial t} + \frac{\partial\rho_s}{\partial p_g}\frac{\partial p_g}{\partial t} + \frac{\partial\rho_s}{\partial\overline{\sigma}}\left[K\left(\nabla\cdot\frac{\partial\mathbf{u}}{\partial t}\right)\right] - 3K\beta\frac{\partial T}{\partial t} - \chi\frac{\partial p_l}{\partial t} - (1-\chi)\frac{\partial p_g}{\partial t}\right] + \frac{\partial\ln(1-n)}{\partial t} + \nabla\frac{\partial u}{\partial t} + \frac{\partial u_i}{\partial t}\frac{\partial(\ln(1-n))}{\partial x_i} = 0 \tag{61}$$

where $\beta_s$ is the thermal expansion coefficient of the solid phase, and $u_i$ is the displacement along direction $i$. The other parameters were defined previously. The determination of $\partial\rho_s/\partial p_l$, $\partial\rho_s/\partial p_g$ and $\partial\rho_s/\partial\overline{\sigma}$ in unsaturated states is a difficult task. In the saturated state, $\partial\rho_s/\partial p_g = 0$, and the values of $\partial\rho_s/\partial p_l$ and $\partial\rho_s/\partial\overline{\sigma}$ are given in [67]. If the bulk modulus of the solid constituent is much larger than the bulk modulus of the porous medium, that is to say, $K_s \gg K$, then the values of $\partial\rho_s/\partial p_l$, $\partial\rho_s/\partial p_g$ and $\partial\rho_s/\partial\overline{\sigma}$ can be assumed to be zero. Eq. (61) can then be simplified as

$$\beta_s\frac{\partial T}{\partial t} + \frac{\partial\ln(1-n)}{\partial t} + \nabla\cdot\frac{\partial\mathbf{u}}{\partial t} + \frac{\partial u_i}{\partial t}\frac{\partial[\ln(1-n)]}{\partial x_i} = 0 \tag{62}$$

## 4. FEM formulation and solution strategy

### 4.1. FEM formulation

The governing equations (18), (27), (40), (48), (51) and (62) are nonlinear differential equations with the following primary variables: displacement (three components), vapor pressure, gas pressure, liquid pressure, porosity and temperature. To solve them, they must be appropriately discretised in space and time. A Galerkin finite element solution approach [68] is used for the spatial discretization. The boundary conditions are introduced into the governing equations naturally. Then the differential governing equations are changed into the numerical matrix equations

$$\mathbf{A}\frac{\partial\mathbf{X}}{\partial t} + \mathbf{B}\mathbf{X} = \mathbf{F} \tag{63}$$

where $\mathbf{A}$ and $\mathbf{B}$ are coefficient matrices, $\mathbf{X}$ is the vector of nodal primary variables, and $\mathbf{F}$ is the vector of nodal loads, expressed by

$$\mathbf{A} = \begin{bmatrix} A_{uu} & 0 & A_{ug} & A_{ul} & A_{uT} & 0 \\ A_{vu} & A_{vv} & A_{vg} & A_{vl} & A_{vT} & A_{vn} \\ A_{gu} & 0 & A_{gg} & A_{gl} & A_{gT} & A_{gn} \\ A_{lu} & 0 & A_{lg} & A_{ll} & A_{lT} & A_{\ln} \\ A_{Tu} & 0 & 0 & 0 & A_{TT} & 0 \\ A_{nu} & 0 & A_{ng} & A_{nl} & A_{nT} & A_{nn} \end{bmatrix}, \quad \mathbf{X} = \begin{bmatrix} \mathbf{U}(t) \\ \mathbf{P}_v(t) \\ \mathbf{P}_g(t) \\ \mathbf{P}_l(t) \\ \mathbf{T}(t) \\ \mathbf{n}(t) \end{bmatrix},$$

$$\mathbf{B} = \begin{bmatrix} 0 & 0 & 0 & 0 & 0 & 0 \\ 0 & B_{vv} & B_{vg} & 0 & B_{lT} & 0 \\ 0 & 0 & B_{gg} & 0 & B_{gT} & 0 \\ 0 & 0 & 0 & B_{ll} & B_{lT} & 0 \\ 0 & 0 & B_{Tg} & B_{Tl} & B_{TT} & 0 \\ 0 & 0 & 0 & 0 & 0 & 0 \end{bmatrix}, \quad \mathbf{F} = \begin{bmatrix} \mathbf{F}_u \\ \mathbf{F}_v \\ \mathbf{F}_g \\ \mathbf{F}_l \\ \mathbf{F}_T \\ 0 \end{bmatrix}.$$

where $\mathbf{U}(t)$, $\mathbf{P}_v(t)$, $\mathbf{P}_g(t)$, $\mathbf{P}_l(t)$, $\mathbf{T}(t)$ and $\mathbf{n}(t)$ are the primary variables of displacement vector (three components), vapor pressure, gas pressure, liquid pressure temperature and porosity, respectively.

The method used for the time discretization is a one-dimensional finite difference scheme. Within each time step, the variation of vectors $\mathbf{X}$ and $\mathbf{F}$ are assumed to follow linear variations, i.e.,

$$\mathbf{X} = N_1\mathbf{X}^{t_k} + N_2\mathbf{X}^{t_k+\Delta t} \tag{63a}$$

$$\mathbf{F} = N_1\mathbf{F}^{t_k} + N_2\mathbf{F}^{t_k+\Delta t} \tag{63b}$$

where $N_1 = 1-\eta$, $N_2 = \eta$, and $\eta = (t-t_k)/\Delta t$. Their time derivatives are then written as

$$\frac{\partial \mathbf{X}}{\partial t} = \frac{\partial N_1}{\partial t}\mathbf{X}^{t_k} + \frac{\partial N_2}{\partial t}\mathbf{X}^{t_k+\Delta t} = \frac{1}{\Delta t}\left[\mathbf{X}^{t_k+\Delta t} - \mathbf{X}^{t_k}\right] \tag{63c}$$

$$\frac{\partial \mathbf{F}}{\partial t} = \frac{\partial N_1}{\partial t}\mathbf{F}^{t_k} + \frac{\partial N_2}{\partial t}\mathbf{F}^{t_k+\Delta t} = \frac{1}{\Delta t}\left[\mathbf{F}^{t_k+\Delta t} - \mathbf{F}^{t_k}\right] \tag{63d}$$

Substituting Eqs. (63a–d) into Eq. (62) then yields the final FEM matrix equation:

$$\left[\mathbf{A}\frac{1}{\Delta t} + \eta\mathbf{B}\right]\mathbf{X}^{t_k+\Delta t} = \left[\mathbf{A}\frac{1}{\Delta t} - (1-\eta)\mathbf{B}\right]\mathbf{X}^{t_k} + \left[1-\eta\right)\mathbf{F}^{t_k} + \eta\mathbf{F}^{t_k+\Delta t}\right] \tag{64}$$

where $\eta$ may take any value from 0 to 1, to generate different time-marching schemes. The values of $\eta = 0$, 0.5 and 1 correspond to the three standard finite difference schemes, i.e., forward difference (Euler), mid-difference (Crank–Nicholson) and backward difference. The value of $\eta = 0.667$ corresponds to the Galerkin difference scheme that is adopted in this paper. In order to start the calculation of Eq. (64), the initial condition is specified as

$$\mathbf{X}^{t_0} = \mathbf{X}_0 \tag{65}$$

### 4.2. Solution strategy

In general, Eq. (64) is a highly nonlinear, asymmetric matrix equation. Many of its diagonal elements are very small in magnitude, which tends to make the coefficient matrix ill-conditioned. In order to solve the matrix equation successfully, two issues need to be addressed. Firstly, a proper equivalent form of the nonlinear differential equations needs to be chosen to keep the desired dominance of diagonal coefficients before FEM discretization. This is necessary to maintain numerical stability and to increase the rate of convergence. Secondly, the coefficients of high nonlinearity are always functions of multiple primary variables, due to the coupling terms in the governing equations. To calculate such highly nonlinear coefficients, the values of the variables should be properly estimated beforehand, using, for example, Eq. (63a). This step is taken to ensure that the final equations describe THM states at the same point in time.

Moreover, if there is a good solution technique that can overcome the difficulties caused by asymmetry and ill-conditioning of the coefficient matrix, such as the one that is used in this paper. It is more efficient to solve the whole matrix equation at the same time as opposed to solve every single equation individually. One of the methods is to divide the whole equation into several groups, and then use an interlaced solution approach with a proper order. Specifically, at each time step the equilibrium equations are solved directly first, followed by direct solution of the liquid flow equations, and the gas and vapor flow equations. The heat equations are solved later, and the solid phase conservation equations are solved last.

## 5. Validation of code by a benchmark test problem

### 5.1. Introduction

The code has been verified through simulating a benchmark test problem, called BMT1, of bentonite tested in laboratory conditions, as defined in WP4 of the THERESA project. The compacted bentonite is planned to be used to limit the flow velocity of groundwater in the near-field of a geological repository for radioactive waste. Water flow and its phase changes, mechanical behavior of the bentonite and the heat produced by the radioactive waste decay make the problem a coupled thermo-hydro-mechanical system. In order to verify the THM computer codes and the constitutive models in the THERESA project, one of three benchmark tests is a laboratory experiment performed on a cylindrical compacted MX-80 bentonite sample by the French Commission of Atomic Energy from 2003 to 2004 [69], the so-called CEA mock-up test.

The samples of bentonite have a diameter and a height of 203 mm (Fig. 1). The bentonite was tightly enclosed in a PTFE sleeve. To minimize heat losses, the cells were insulated with a heat-proof envelope. The experiments were not gas tight, however. Heat was applied at the bottom plate, whereas hydration proceeds from the top of the samples. Two different initial water contents were used to manufacture the samples. Each test was composed of two phases. In Phase 1, heat was applied to one end of the cylinder, while the temperature at the other end was kept constant and equal to 20 °C. A maximum temperature of 150 °C was applied. Phase 2 started after thermal equilibrium was achieved, and involved the gradual hydration of the samples. A constant water pressure was applied to the end opposite the one where the temperature variation was prescribed. Constant volume conditions were ensured in the two phases of the test. The main variables that were measured during the tests include temperatures, relative humidity, total axial stress and total radial stress. In the following part of this section, the simulation of the CEA benchmark test by the new code is presented for comparison with the measured results.

Considering the detailed physical processes of benchmark tests and the definitions of WP4 of THERESA project, a nonlinear elastic stress–strain relation, Eq. (19), was used in the simulation of benchmark tests, mainly because the compacted bentonite was confined in a small space, and the deformation was very small. It was felt that for these particular conditions, a more elaborate inelastic stress–strain law was not necessary.

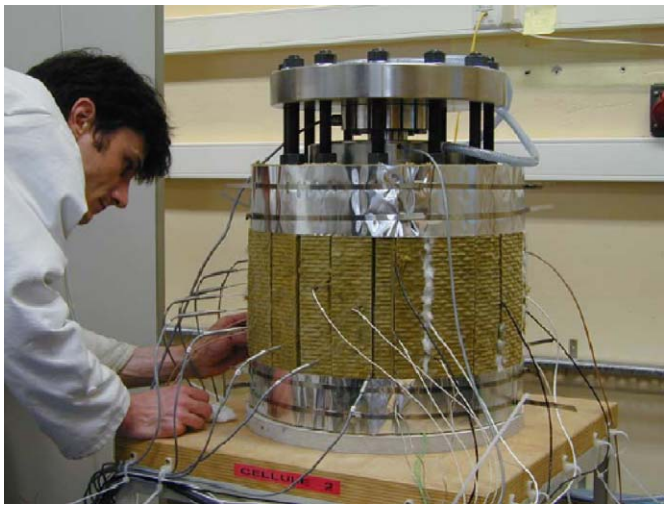

**Fig. 1.** Bentonite THM mock-up experiment.

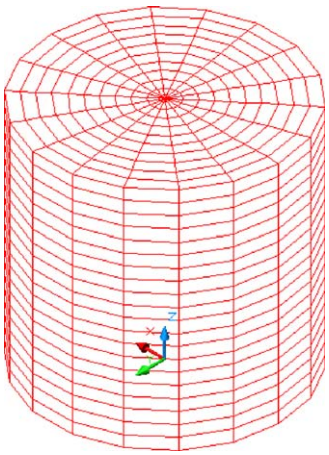

**Fig. 2.** The 3-D FEM mesh.

### 5.2. Numerical model

#### 5.2.1. The FEM model geometry

The model geometry is the same as the samples, with the diameter and the height each equal to 203 mm. Hexahedron elements have been used to build the 3D FEM mesh (Fig. 2). The total number of nodes is 671. The total number of elements is 600.

#### 5.2.2. Boundary conditions

The temperature variation at the bottom end of the model is as specified during the test; it was raised in steps until reaching 150 °C. The temperature at the top end of the specimen was kept constant at 20 °C. The other surfaces are adiabatic.

According to the test procedure, the hydraulic boundary condition is impermeable for all surfaces of the model in the first phase. In the second phase, the pore water pressure at the top of the model is held constant at 1.0 MPa. The other surfaces are impermeable. The gas pressure is equal to the atmospheric pressure on the top surface of the model. Mechanically, the boundary surfaces are fixed in their normal directions as roller boundaries.

#### 5.2.3. Initial conditions

The initial values were obtained according to the measured data from the definition of BMT1 (bentonite THM mock-up experiments [69]). The initial values of porosity, relative humidity and degree of saturation are 0.3242, 0.6 and 0.755, respectively. Initial temperature is 20 °C. Initial gas pressure is 0.10132 MPa, and the initial stress of sample is 0.5 MPa.

#### 5.2.4. The main material parameters

According to the measured data from the definition of BMT1 (the bentonite THM mock-up experiments [69] and other relevant papers [34,70]), the values of material parameters were set for the simulation. The intrinsic permeability is $1.0E-21\ m^2$. Thermo-osmosis coefficient of liquid is $7.0E-12\ m^2/s\ K$. The specific heat capacity of solid is 920 J/kg, and the thermal expansion coefficient of solid is $1.0E-5\ 1/K$. Other parameters are presented previously.

### 5.3. Results and interpretations

#### 5.3.1. Comparison of measured and simulated result

*Temperature*: Fig. 3 shows the comparison between measured and simulated temperature as a function of time. At the bottom end of the sample, the measured and simulated temperatures agree well (from the top of the sample to the bottom, the sensors are $T_0$, $T_1$, $T_2$, $T_3$,…,$T_{13}$, $T_{14}$, respectively). At the top end of the sample, the simulation underestimates the temperature slightly at the initial heating stage, but the trends generally agree well.

*Axial stress*: The measured results of radial stress have certain uncertainties during the experiment and therefore cannot be used for code verification. Consequently, we only give the comparison between measured and simulated results of the axial stress (Fig. 4). The general behaviors of the measured and simulated results are almost the same, and the discrepancies in magnitude are small or moderate. Reasons for the slight differences may be that the assumed mechanical parameters may not be accurate enough to represent the actual behavior of the bentonite tested, according to the interpretation of the laboratory test analysis in WP4, and the adopted swelling pressure model may not be sufficiently realistic.

*Relative humidity and vapor pressure*: Before giving the simulated results, it is necessary to clarify the difference between our approach and the ones used by others in calculating the relative humidity and vapor pressure. In some THM models, the vapor flow equation is neglected. In such cases, the simulated results exclude the effect of vapor pressure; thus, the calculation of relative humidity RH must depend on empirical models, for example, [22,71,72]:

$$RH = \exp(\alpha s/\rho_l R_v T) \tag{66}$$

where $s$ is the suction, $\rho_l$ is the density of water, $R_v$ is the specific gas constant for water vapor, $T$ is the temperature, and $\alpha$ is an empirical coefficient.

In our approach, the THM model includes the vapor flow equation, and vapor pressure is adopted as a primary variable that can be obtained directly. Thus, the relativity humidity can be calculated simply and directly by adopting its physical definition, without relying on empirical models, as given by

$$RH = \frac{p_v}{p_{sv}} \times 100\% \tag{67}$$

where $p_v$ is the vapor pressure, and $p_{sv}$ is the saturated vapor pressure.

The simulated results of the vapor pressure are shown in Fig. 5. Although there are no measured results with which to compare, it shows that the variation of vapor pressures is realistic, to some extent. Fig. 6 shows a comparison between measured and simulated results of relative humidity versus time. The general trends between measured and simulated results agree well, with marginal differences in magnitude. The reason for such small discrepancies may be that the adopted thermo-osmosis coefficient and accommodation coefficient, both of which are taken to be constant, cannot account for the influence of saturation degree during the test as functions of temperature and pressure.

#### 5.3.2. Discussion

The general agreement between the simulated and measured results of the benchmark test indicates that the coupled THM processes can be well simulated by the fully coupled thermo-hydro-mechanical numerical models.

The good agreement between the simulated and measured temperature indicates that the model can simulate the thermal response of processes having high temperature gradients. Numerical simulation shows that the thermal conductivity of bentonite, treated as a mixture of three material phases, plays an important role in the thermal response of the whole medium. The numerical results can be further improved if the effects of the material heterogeneity can be quantified during testing.

The evolution of the relativity humidity was well predicted both in trends and magnitudes. It indicates that the model can

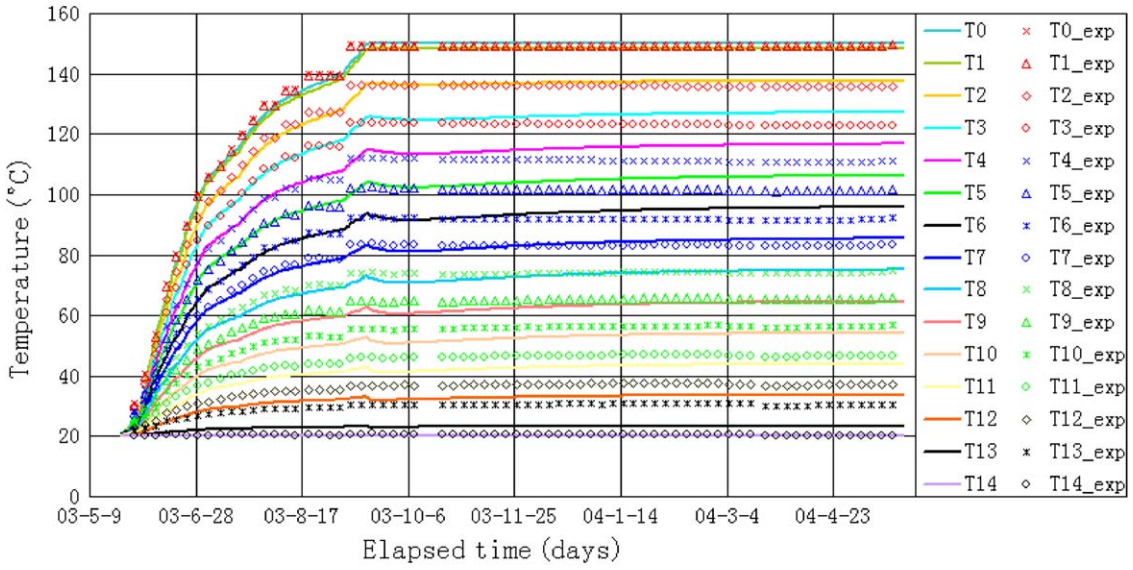


**Fig. 3.** Comparison of results between the simulated and measured temperature at different locations (heights) of the specimen as functions of time.

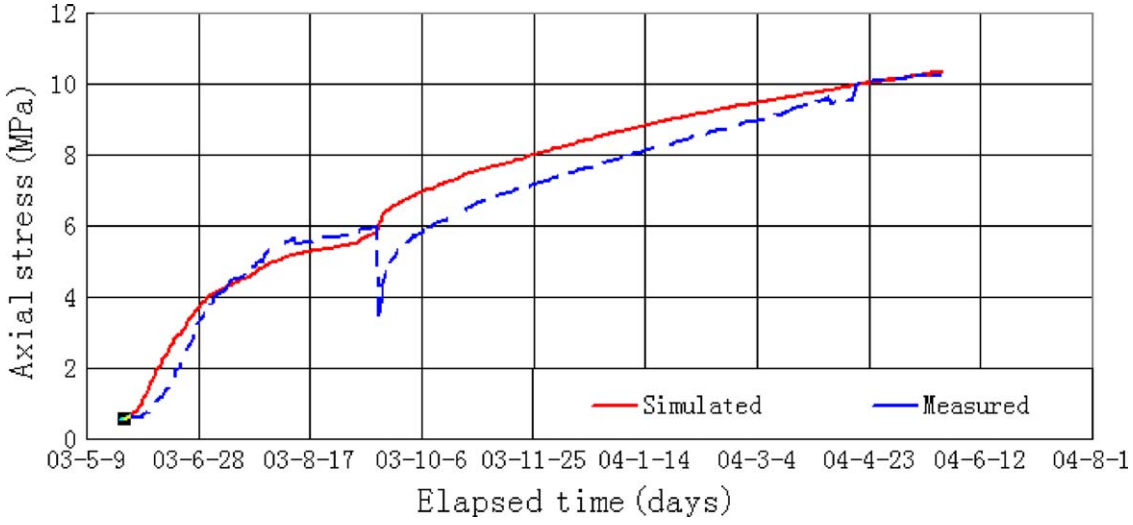


**Fig. 4.** Comparison of results between simulated and measured axial stress vs. time.

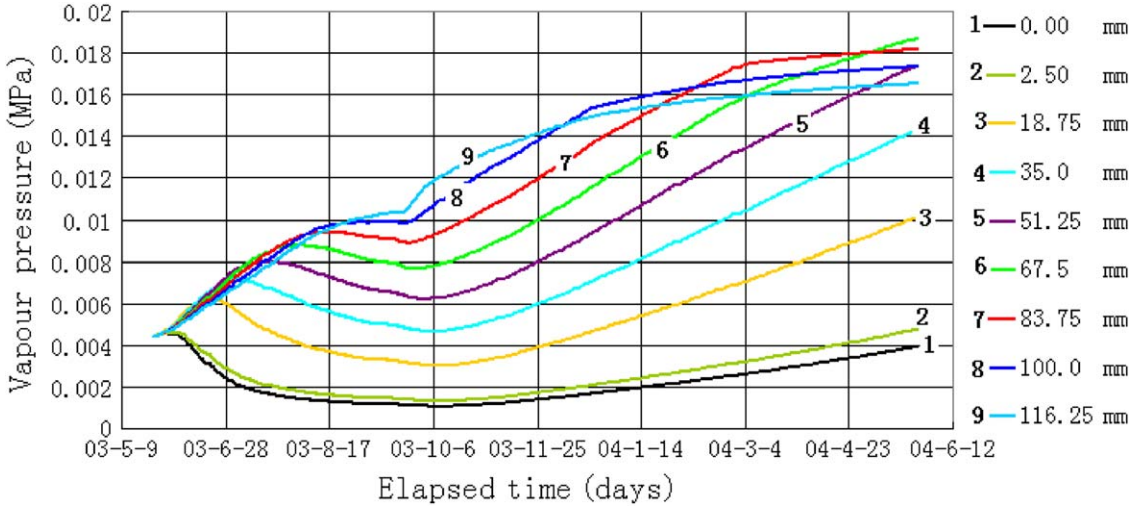


**Fig. 5.** The simulated results of vapor pressure.

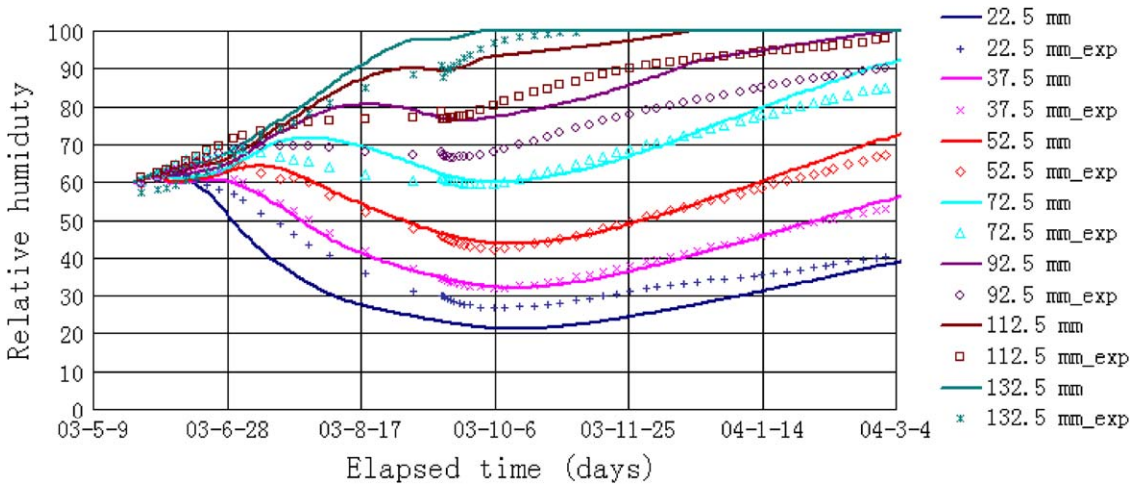


**Fig. 6.** Comparison between simulated and measured relative humidity.

predict liquid flow, gas flow, vapor flow and heat flow with high confidence, because the relative humidity depends highly on suction, gas pressure, vapor pressure and temperature. Since the equations governing the gas flow and vapor flow are intrinsic components of the model, some assumptions that are often used in different approaches, such as the assumptions of the empirical model of relative humidity and the assumption of a constant and small gas pressure, are unnecessary here, and the model becomes more comprehensive and reliable.

The evolution of the axial stress was also reasonably well simulated, in trend and magnitude. Numerical calculation shows the results of stress strongly depend on the thermal expansion coefficient, swelling pressure, and the constitutive relationship between stress and strain. More comprehensive development of the material models is needed to further improve the code's numerical capability, such as elastoplastic models of the Cam clay type, for example.

In addition, the porosity was shown to be an important parameter that plays an indispensable role in interactions between solid and fluid phases, although the change in its value is always small. The numerical analysis shows that it affects the stability and efficiency of the numerical simulations to a significant extent, especially in the case of appearance of an abrupt deformation gradient, such as would occur after a sudden application of external loads.

Finally, although the model is complete and compact in terms of governing equations, this in itself does not necessarily lead to realistic and accurate simulated results. Care should be taken to discretize the gas flow and vapor flow equations to improve the solution stability and the astringency because of the fact that their coupling with deformation process often leads to ill-conditioning of the FEM coefficient matrix. Our approach for avoiding the ill-conditioning is to use, before FEM discretization, the equivalent form of the gas and vapor flow equations that can maintain the diagonal dominance of the main coefficient matrix, but better techniques should be investigated to improve our numerical solution capabilities. In essence, a robust equation solver is the final link that produces desired results with reliability of the model and results.

## 6. Concluding remarks

The presented mathematical theory of mixtures, FEM formulation and solution technique are demonstrated to be comprehensive and reliable tools for simulating fully coupled thermo-hydro-mechanical processes of multiphase geological media, which is essential for performance and safety assessments of geological waste repositories. The use of the theory of mixture makes the simulation of the coupled THM processes more process-oriented, without the need for using empirical models for unsaturated fluid flow under non-isothermal conditions, which is often a challenging task. This, however, does not mean that commonly used phenomenological Biot theory for poroelasticity or poro-elasto-plasticity cannot achieve the same objectives with similar or better solutions. We found that although the completeness and compactness of the governing equations are necessary conditions to properly represent the behaviors of the three phases (solid, liquid and gas) according to the first principles of thermodynamics for multiphase porous media, an efficient and robust solution technique is a necessary condition to yield meaningful results as the final product. This is due to the fact that coupled THM processes produce a highly nonlinear FEM coefficient matrix, due to the coupling terms, and thereby generate a significant degree of ill-conditioning.

A key issue in modeling multiphase THM behavior of deformable porous media is that some of the key components we need most, such as the water retention model and the definition and measurement of the relative humidity, often rely on empirical relations whose predictions may or may not be physically reliable or consistent for the former, and difficult to measure directly and accurately for the latter. In this regard, the theory of mixtures for multiphase flow may be a useful alternative tool to reduce such difficulties to a limited extent. Our approach presented in this paper is only an attempt to investigate such a possibility. Alternative and better techniques may certainly exist.

The presented model is the result of the initial stage of the THERESA project. Further work is underway for developing bentonite and rock interface models, more comprehensive constitutive models of bentonite and rocks, more code verifications against laboratory and field scale experiments, and continued improvements of the solution technique.

## Acknowledgments

The work performed in this paper is sponsored by the European Commission through the THERESA project. The authors are grateful for fruitful discussions with our THERESA project

partners and Dr. Yifeng Chen from Wuhan University, China. The authors also appreciate very much the support to this research of professors Tian Bin and Defu Liu of China Three Gorges University.

## References


[1] von Terzaghi K. Die berechnug der Durchlässigkeitsziffer desTones aus dem Verlauf der hydrodynamischen Spannungserscheinungen. Sitzungsber Akad Wiss Math-Naturwiss Section IIa 1923;132(3/4):125–38.

[2] Biot MA. General theory of three-dimensional consolidation. J Appl Phys 1941;12:155–64.

[3] Biot MA. General solution of the equation of elasticity and consolidation for a porous material. J Appl Mech 1956;23:91–6.

[4] Morland LW. A simple constitutive theory for fluid saturated porous solids. J Geophys Res 1972;77:890–900.

[5] Bowen RM. Compressible porous media models by use of theories of mixtures. Int J Eng Sci 1982;20:697–735.

[6] Hassanizadeh M, Gray WG. General conservation equations for multiphase systems: 1. Averaging procedures. Adv Water Resourc 1979;2:131–44.

[7] Hassanizadeh M, Gray WG. General conservation equations for multiphase systems: 2. Mass momenta, energy and entropy equations. Adv Water Resourc 1979;2:191–203.

[8] Hassanizadeh M, Gray WG. General conservation equations for multiphase systems: 3. Constitutive theory for porous media flow. Adv Water Resourc 1980;3:25–40.

[9] Hassanizadeh M, Gray WG. Mechanics and theormodynamics of multiphase flow in porous media including interphase transport. Adv Water Resourc 1990;13:169–86.

[10] Achanta S, Cushman JH, Okos MR. On multicomponent, multiphase thermomechanics with interfaces. Int J Eng Sci 1994;32:1717–38.

[11] de Boer R. The thermodynamic structure and constitutive equations for fluid-saturated compressible and incompressible elastic porous solids. Int J Solids Struct 1998;35(34–35):4557–73.

[12] Jing L. A review of techniques, advances and outstanding issues in numerical modeling for rock mechanics and rock engineering. Int J Rock Mech Min Sci 2000;40:79–87.

[13] Noorishad J, Tsang C-F. ROCMAS-simulator: a thermohydromechanical computer code. In: Stephansson O, Jing L, Tsang C-F, editors. Coupled thermo-hydro-mechanical processes of fractured media. Amsterdam: Elsevier; 1996. p. 551–8.

[14] Ohnishi Y, Kobayashi A. THAMES. In: Stephansson O, Jing L, Tsang C-F, editors. Coupled thermo-hydro-mechanical processes of fractured media. Amsterdam: Elsevier; 1996. p. 545–59.

[15] Nguyen TS. Description of the computer code FRACON. In: Stephansson O, Jing L, Tsang C-F, editors. Coupled thermo-hydro-mechanical processes of fractured media. Amsterdam: Elsevier; 1996. p. 539–44.

[16] Börgesson L. ABAQUS. In: Stephansson O, Jing L, Tsang C-F, editors. Coupled thermo-hydro-mechanical processes of fractured media. Amsterdam: Elsevier; 1996. p. 565–70.

[17] Thomas HR, He Y, Sansom MR, Li CLW. On the development of the thermo-mechanical-hydraulic behaviour of unsaturated soil. Eng Geol 1996;41:197–218.

[18] Olivella S, Carrera J, Gens A, Alonso EE. Nonisothermal multiphase flow of brine and gas through saline media. Transp Porous Media 1994;15:271–93.

[19] Richards LA. Capillary conduction of liquids through porous media. Physics 1931;1:318–33.

[20] Rutqvist J, Börgesson L, Chijimatsu M, et al. Thermohydromechanics of partially saturated geological media: governing equations and formulation of four finite element models. Int J Rock Mech Min Sci 2001;38:105–27.

[21] Khalili N, Loret B. An elasto-plastic model for non-isothermal analysis of flow and deformation in unsaturated porous media: formulation. Int J Solids Struct 2001;38:8305–30.

[22] Schrefler BA, Pesavento F. Multiphase flow in deforming porous material. Comput Geotech 2004;31:237–50.

[23] Truesdell C, Toupin R. The classical field theories. In: Flugge S, editor. Handbuch der Physik. Berlin: Springer; 1960. p. 226–793.

[24] Bear J, Bachmat Y. Introduction to modeling of transport phenomena in porous media. Dordrecht: Kluwer; 1991 553 pp.

[25] Bowen RM. Theory of mixtures. In: Eringen AC, editor. Continuum Physicsphysics, vol. III. New York: Academic Press; 1976. p. 1–127.

[26] Li WM, Rubin D, Krempl E. Introduction to continuum mechanics. Oxford: Pergamon; 1993 571 pp.

[27] Lewis RW, Schrefler BA. The finite element method in the static and dynamic deformation and consolidation of porous media. Chichester: Wiley; 1998 492 pp.

[28] Eringen AC, Ingram JD. A continuum theory for chemically reacting media–I. Int J Eng Sci 1965;3:197–212.

[29] Nur A, Byerlee JD. An exact effective stress law for elastic deformation of rock with fluids. J Geophys Res 1971;76(26):6414–9.

[30] Bishop AW. The principle of effective stress. Teknisk Ukeblad 1959;106(39):859–63.

[31] Jennings JEB, Burland JB. Limitation to the use of effective stress in unsaturated soils. Geotechnique 1962;12(2):125–44.

[32] Bishop AW, Blight GE. Some aspects of effective stress in saturated and partly saturated soils. Geotechnique 1963;13:177–97.

[33] Burland JB. Some aspects of the mechanical behaviour of partly saturated soils. In: Proceedings of the symposium on moisture equilibria and moisture changes in the soils beneath covered areas. Sydney: Butterworths; 1965. p. 270–8.

[34] Loret B, Khalili N. A three phase model for unsaturated soils. Int J Numer Anal Meth Geomech 2000;24:893–927.

[35] Carslaw HS, Jaeger JC. Conduction of heat in solids, 2nd ed. Oxford: Oxford University Press; 1959 510510 pp.

[36] Alonso EE, Gens A, Josa A. A constitutive model for partially saturated soils. Géotechnique 1990;40:405–30.

[37] Lore B, Khalili N. An effective stress elastic-–plastic model for unsaturated porous media. Mech Maters 2002;34:97–116.

[38] Khalili N, Khabbaz MH. A unique relationship for $\chi$ for the determination of the shear strength of unsaturated soil. Géotechnique 1998;48(5):681–7.

[39] Rao SM, Thyagaraj T. Role of direction of sal migration on the swelling behaviour of compacted clays. Appl Clay Sci 2007;38:113–29.

[40] Barbour SL, Fredlund DG. Mechanisms of osmotic flow and volume change in clay soils. Can Geotech J 1989;26:551–62.

[41] Musso G, Romero ME, Gens A, Castellanos E. The role of structure in the chemically induced deformations of FEBEX bentonite. Appl Clay Sci 2003;23:229–37.

[42] Peters GP, Smith DW. The influence of advective transport on coupled chemical and mechanical consolidation of clays. Mech Maters 2004;36:467–486.

[43] Villar MV. Thermo-hydro-mechanical characterization of a bentonite from Cabo de Gata. A study applied to the use of bentonite as sealing material in high level radioactive waste repositories, 2002.

[44] Walczak RT, Moreno F, Slawinski C, et al. Modeling of soil water retention curve using soil solid phase parameters. J Hydrol 2006;329:527–33.

[45] Nuth M, Laloui L. Advances in modeling hysteretic water retention curve in deformable soils. Comp Geotech 2008;35:835–44.

[46] Pires LF, Cassaro FAM, Reichardt K, et al. Soil porous system changes quantified by analyzing soil water retention curve modifications. Soil Tillage Res 2008;100:72–7.

[47] Hwang S, Choi S. Use of a lognormal distribution model for estimating soil water retention curve from particle-size distribution data. J Hydrol 2006;323:325–34.

[48] Romero E, Gens A, Loret A. Water permeability, water retention and microstructure of unsaturated compacted Boom clay. Eng Geol 1999;54:117–27.

[49] Villar MV, Martin PL, Barcala JM. Infiltration tests at isothermal conditions and under thermal gradient. Technical Report CIEMAT/DMA/M2140/1/05, Madrid, 2005, 24 pp.

[50] Hadas A. Deviations form Darcy's law for the flow of water in unsaturated soils. Isr J Agr Res 1964;14(4):159–68.

[51] Delshad M, Pope GA. Comparison of the three-phase oil relative permeability models. Transp Porous Media 1989;4:59–83.

[52] Burdine NT. Relative permeability calculations from pore size distribution data. Trans AIME 1953;198:71–8.

[53] Avraam DG, Payatakes AC. Generalized relative permeability coefficients during steady-state two-phase flow in porous media. Transp Porous Media 1995;20:135–68.

[54] Stallman, RW. Multiphase fluid flow in porous media—a review of theories pertinent to hydrologic studies. US Geol Surv, paper no. 411-E, 1964, 51 pp.

[55] Roitburd AL. Modified Clausius–Clapeyron equation for hysteresis of phase transformation in solids. Fiz Tverd Tela 1983;25(1):33–40.

[56] Guvanasen V, Chan T. A three-dimensional numerical model for thermo-hydromechanical deformation with hysteresis in a fractured rock mass. Int J Rock Mech Min Sci 2000;37:89–106.

[57] Laloui L, Klubertanz G, Gulliet L. Solid–liquid–air coupling in multiphase porous media. Int J Numer Anal Meth Geomech 2003;27:183–206.

[58] Dana E, Skoczylas F. Gas relative permeability and pore structure of sandstones. Int J Rock Mech Min Sci 1999;36:613–25.

[59] Feng H, Tang J, et al. Intrinsic and relative permeability for flow of humid air in unsaturated apple tissues. J Food Eng 2004;62:185–92.

[60] Oak MJ, Baker LE, Thomas D. Three-phase relative permeability of Berea sandstone. J Petrol Tech 1990;42(8):1054–61.

[61] Crane. Flow of fluids through Valves, fittings and Pipe. Technical paper No. 410, 1988. Crane Company, Joliet, Illinois.

[62] Tang AM, Cui YJ, Le TT. A study on the thermal conductivity of compacted bentonites. Appl Clay Sci 2008;41:181–9.

[63] Sakashita H, Kumada T. Heat transfer model for predicting thermal conductivity of highly compacted bentonite. J Jap Atom Soc 1998;40:235–40.

[64] Sepaskhan AR, Boersma L. Thermal conductivity of soils as a function of temperature and water content. Soil Sci Soc Am J 1979;43:439.

[65] Becker BR, Misra A, Fricke BA. Development of correlations for soil thermal conductivity. Int Commun Heat Mass Transfer 1992;19:59–68.

[66] Abu-Hamdeh NH, Khdair AI, Reeder RC. A comparison of two methods used to evaluate thermal conductivity for some soils. Int J Heat Mass Transfer 2001;44:1073–8.

[67] Zimmerman RW. Coupling in poroelasticity and thermoelasticity. Int J Rock Mech Min Sci 2000;37:79–87.

[68] Zienkiewicz OC, Taylor RL. The finite element method, vol. 1, Basic formulations and linear problems, 5th ed. London: Butterworth-Heinemann; 2000.
[69] Gatabin C, Billaud P. Bentonite THM mock up experiments. Sensor data report. CEA, Report NT-DPC/SCCME 05-300-A, 2005.
[70] Marshall TJ, Holmes JW. Soil physics. Bristol: Cambridge University Press; 1988, 319 pp.
[71] Villar MV, Garcia-Sineriz JL, Barcena I, et al. State of the bentonite barrier after five years operation of an in situ test simulating a high level radioactive waste repository. Eng Geol 2005;80: 175–98.
[72] Nguyen TS, Selvadurai APS, Armand G. Modelling the FEBEX THM experiment using a state surface approach. Int J Rock Mech Min Sci 2005;42:639–51.